Journal of The Electrochemical Society, **158** (6) C165-C171 (2011)
0013-4651/2011/158(6)/C165/7/$28.00 © The Electrochemical Society

ToF-SIMS Imaging Study of the Early Stages of Corrosion in Al-Cu Thin Films

A. Seyeux,[a,z] G. S. Frankel,[b,*] N. Missert,[c,] K. A. Unocic,[d] L. H. Klein,[a] A. Galtayries,[a] and P. Marcus,[a,z]**

[a]*Laboratoire de Physico-Chimie des Surfaces, Ecole Nationale Supérieure de Chimie de Paris, Chimie ParisTech, ENSCP/CNRS (UMR 7045), Paris 75005, France*
[b]*The Ohio State University, Columbus, Ohio 43210, USA*
[c]*Sandia National Laboratories, Albuquerque, New Mexico 87185, USA*
[d]*Oak Ridge National Laboratory, Oak Ridge, Tennessee 37381, USA*

The pitting corrosion of Al-Cu thin film alloys was investigated using samples that were heat treated in air to form through-thickness Al_2Cu particles within an Al-0.5% Cu matrix. Time-of-Flight Secondary Ion Mass Spectroscopy (ToF-SIMS) analysis revealed Cu-rich regions 250–800 nm in lateral extent near the metal/oxide interface. Following exposure that generated pitting corrosion, secondary electron, secondary ion, and AFM images showed pits with size and density similar to those of the Cu-rich regions. The role of the Cu-rich regions is addressed.
 [DOI: 10.1149/1.3568944]

Manuscript submitted November 23, 2010; revised manuscript received February 23, 2011. Published March 31, 2011.

Aluminium alloys are widely used in aerospace applications due to their very good mechanical properties, low densities and good uniform corrosion resistance. Copper is one of the most common alloying elements and a variety of alloys in which copper is the major addition have been developed. Due to the low solid solubility of copper in aluminium, the aging of Al-Cu alloys under high temperature conditions leads to the formation of intermetallic Cu-rich particles, including θ-phase Al_2Cu, that are known to lead to pitting corrosion susceptibility in aqueous chloride environments.[1–12]

The Cu-rich particles in Al alloys can play several roles that might promote localized corrosion. They are known to have higher potentials than the bulk matrix so that galvanic interaction with the matrix might increase the local potential above the breakdown potential.[3,4,6,10,11,13–15] The oxide on these particles might be more conductive or catalytic, thereby providing more cathodic current from oxygen reduction that can drive localized corrosion.[3,4,11,13,15,16] The local higher rate of oxygen reduction can lead to local *p*H changes that attack the neighboring matrix, causing trenching and/or Cu enrichment.[12,17–19] The interface between particles and matrix can also provide initiation sites for localized attack due to local disorder at the phase boundary.[20]

Model thin film alloys with nanoscale surface roughness allow a detailed investigation of local morphology, microstructure and composition that may influence pit initiation. Thin film and bulk Al-Cu alloys were used as model samples in this work. Prior experiments on thin film Al-Cu samples found that rapid anodic corrosion of the matrix could be initiated at the open circuit potential at a pre-existing defect in a near neutral solution of 0.01 M NaCl + 0.3% vol H_2O_2. Pitting corrosion near the theta phase intermetallic particles was observed in the cathodic regions where the *pH* increased as evidenced by confocal scanning laser microscopy in the presence of a *p*H indicator. However, pitting corrosion was observed only at some of the particles in the high *p*H region.[21]

Time-of-Flight Secondary Ion Mass Spectroscopy (ToF-SIMS) was used in this study to investigate whether compositional heterogeneities existed in the oxide covering the Al_2Cu particles or the matrix, in both thin film and bulk samples. The goal was to assess whether compositional heterogeneity in the oxide above the particles could be related to differences in local reactivity. Although XPS and Auger spectroscopies have been previously used to observe the presence of metallic Cu in the oxide above model Al_2Cu alloys,[4,13] the sensitivity of these techniques and the spatial resolution of XPS are limited. Recent ToF-SIMS imaging of Cu in corrosion product surrounding intermetallic particles in Al alloys has allowed the spatial extent of Cu redistribution to be measured.[22]

Experimental

Material synthesis and exposures.—The thin films were prepared by depositing 100 nm of Al-Cu (with Cu content equal to 3.5 or 7 wt %) on SiO_2/Si substrates. The deposition treatment consisted of electron-beam co-evaporation from 99.9999% Al and 99.99% Cu sources at room temperature with the rates adjusted and to give the desired composition. A surface oxide layer was formed by exposure to pure oxygen for several hours. Samples were then aged in air at 300°C for 10 h followed by 450°C for 5 min in order to form Al_2Cu intermetallic particles in an Al-0.5 wt % Cu matrix.

A bulk sample of Al-Cu alloy was investigated for comparison. The alloy was melted from pure alloy stock and contained 4 wt % Cu. It was heated at 560°C for 1 h to create a homogeneous Al-Cu solid solution, water quenched, polished to 1 μm diamond paste, and then aged in air using the same temperatures and times described above.

Thin film samples were analyzed by ToF-SIMS in one of three conditions: (a) thermal treatment only, (b) 30 min immersion at the open-circuit potential to a near neutral electrolyte containing 0.01 M NaCl + 0.3% vol H_2O_2 where pitting was not initiated at a pre-existing defect, and (c) 30 min immersion at the open-circuit potential to 0.01 M NaCl with the *p*H adjusted to 11.5 with NaOH in order to obtain the same pitting morphology previously observed in cathodic regions of the electrode during rapid anodic pitting at a pre-existing defect.[21] These samples will be referred to as A, B, and C throughout the manuscript. ToF-SIMS analysis of the bulk sample was also performed, and will be referred to as sample D. Note that identical corrosion morphology was observed for both Al-3.5% Cu and Al-7% Cu thin films exposed to *p*H 11.5. For 30-min exposures, the oxide remained passive except for localized pitting.

ToF-SIMS, AFM, and FIB analyses.—ToF-SIMS analyses were performed using a ToF-SIMS V spectrometer (ION TOF GmbH – Munster, Germany). The analysis chamber was maintained at less than 1.10^{-9} Pa. A pulsed 25 keV Bi^+ primary ion source was employed for analysis. The total primary ion flux was below 10^{12} ions/cm^2 to ensure static conditions. Depth profiles were acquired using a Cs^+ sputter beam. Data acquisition and post-processing analyses were performed using the Ion-Spec commercial software.

Atomic Force Microscopy (AFM) imaging in acoustic AC mode (i.e. tapping mode in which the tip is excited in acoustic way at its resonance frequency) was performed in air, at room temperature using a Agilent 5100 microscope (Agilent Technologies). Topographic AFM

* Electrochemical Society Fellow.
** Electrochemical Society Active Member.
z E-mail: antoine-seyeux@chimie-paristech.fr; philippe-marcus@chimie-paristech.fr

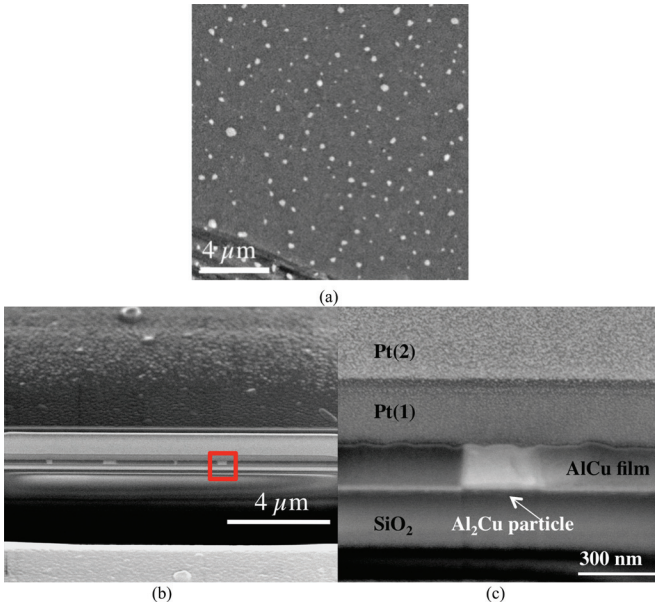

Figure 1. (Color online) SEM micrographs of an Al-3.5 wt % Cu thin film after the thermal treatment. (a) Top view showing distribution of sub-micron Al_2Cu particles (b) FIB cross-section of film (c) detailed view of the area marked on (b).

images of the surface were acquired (mapping of the relief of the surface in x, y and z directions). Stiff SiN type cantilevers from Applied Nanostructures, with a force constant of 50 N/m and a tip radius lower than 10 nm were employed.

Cross sections and SEM images of the thin films were obtained with a FEI Helios Nanolab 600, while the bulk sample sectioning and imaging was performed using a FEI Nova 600 dual beam focus ion beam (FIB) instrument. In both cases, the surface of the sample was protected from damage due to Ga ion milling by depositing a thin Pt layer.

Results

Thin film samples.—As shown in Fig. 1a, the thin film samples exhibited a microstructure after aging that consisted of a distribution of Al_2Cu (θ phase) particles in an Al-rich matrix that had less than 0.5% Cu according to EDS measurements. Figures 1b and 1c show SEM micrographs of a FIB cross section cut in the deposited layer. The particles were through-thickness, and had diameters ranging between ~20 and 300 nm. They were identified as Al_2Cu by selected area electron diffraction analysis obtained on plan view TEM specimens.

The thin film sample B, which was exposed to near neutral 0.01 M NaCl + 0.3% vol H_2O_2 for 30 min after the thermal treatment, did not exhibit evidence of localized corrosion. Pitting corrosion was observed for the sample C, which was exposed for 30 min to 0.01 M NaCl adjusted to *p*H 11.5. The *p*H was increased in this exposure to simulate the environment expected in the high *p*H cathodic regions.

Figure 2 presents a typical ToF-SIMS negative ion depth profile of the unexposed sample A. The depth profile observed for sample B was almost identical. In Fig. 2, the counts associated with the Al-containing ions (Al^-, AlO^-, AlO_2^-, Al_2^-), Si-containing ions (Si^-, SiO_2^-), $^{63}Cu^-$, OH^- and $^{18}O^-$ ions, all recorded simultaneously, are plotted versus Cs^+ ion sputtering time. The $^{16}O^-$ intensity saturated the detector, so the signal of the isotope $^{18}O^-$ is plotted instead. The AlO_2^- and Al_2^- signals are representative of the aluminium oxide and the metallic substrate, respectively. Note that the intensity is reported using a logarithmic scale, which emphasizes the low intensity signals. The changes in secondary ion (SI) intensity with the sputter time reflect in-depth variations in concentration, but they are also strongly dependent on the matrix from which the ions are emitted.

Three main regions can be identified in Fig. 2. The first one, corresponding to the first 40 s of sputtering, is characterized by high intensity and relatively constant AlO^-, AlO_2^- and $^{18}O^-$ signals. This region is assigned to the presence of an oxide film formed on the deposited alloy film after exposure to oxygen for several hours and exposure to air during the thermal treatment. No CuO^- (not shown on Fig. 2 for clarity) or Cu^- signal can be detected in this region,

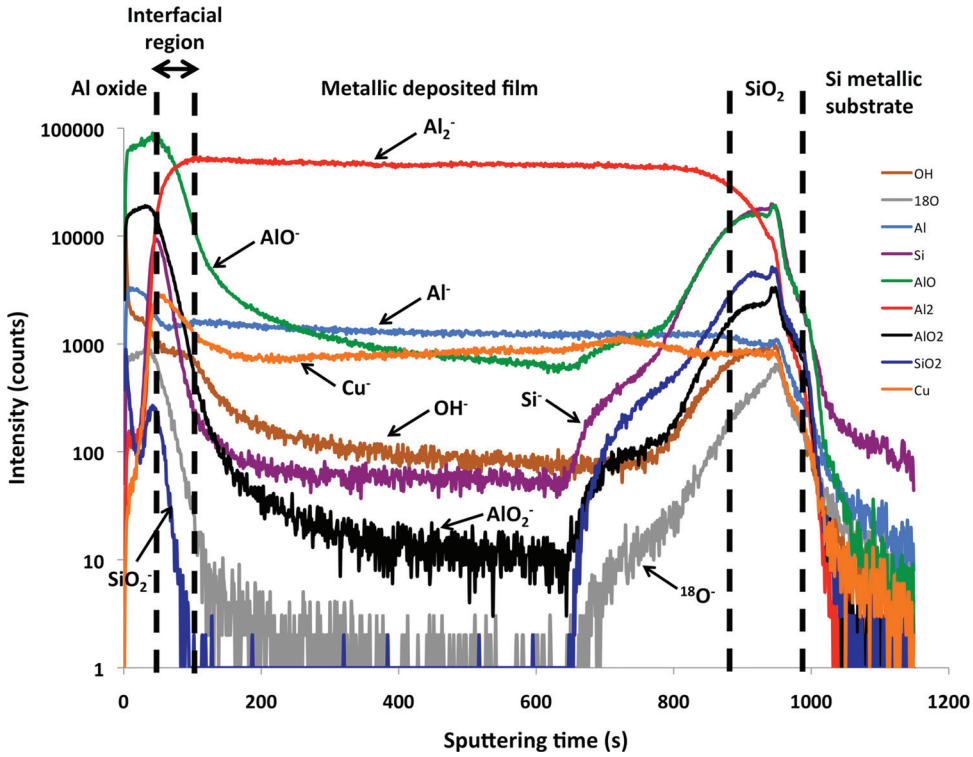

Figure 2. (Color online) ToF-SIMS negative ion depth profile obtained on thin film Al-3.5 wt % Cu sample A. The oxide film, the metallic film and the Si substrate are indicated on the profile.

which indicates that an aluminium oxide layer (Al_2O_3) is formed. Note that in this approach, the signal is from an area of 100×100 μm^2 with no further spatial resolution, so oxide above both the matrix and θ phases contributes to the total signal. The average thickness of the aluminium oxide film can be estimated to be 7 nm assuming an oxide density of 2.34×10^{22} atom cm^{-3} and a sputter yield of ~1.5, which is the sputter yield of metallic Al. After about the first 40 s of sputtering, the intensities of the AlO^-, AlO_2^- and $^{18}O^-$ ions start to decrease and the Al_2^- intensity signal increases drastically indicating the start of the Al oxide/metallic Al deposited film interface region in the depth profile that is mainly due to the surface roughness. After another 40 s of sputtering, the large and constant Al_2^- signal indicates the second region associated with the metallic deposited layer. After about 875 s of total sputtering, the Al_2^- intensity signal starts to drop, whereas Si signals (Si^- and SiO_2^-) and $^{18}O^-$ signal reach high intensity. This indicates that the metallic deposited film/Si substrate interface is reached (the position of the interface and thus the thickness of the metallic deposited film can be estimated from the intensity plateau on the Al_2^- signal). The high SiO_2^- signal that reaches its maximum intensity after around 950 s of total sputtering indicates that a thin layer of silicon oxide covers the Si substrate. After 980 s of sputtering, one enters the Si substrate.

Figure 2 shows a clear peak in the $^{63}Cu^-$ signal at the oxide/metal interface region before decreasing to the stable value in the metallic region. Note that no CuO^- signal was observed, even within the metal/oxide interfacial region. This type of Cu enrichment at the metal-oxide interface has been previously observed on Al_2Cu thin films[23] and Al-low weight percent Cu thin films[24,25] using Rutherford backscattering. To investigate this region further, ToF-SIMS mapping was performed on samples A and B, which gave essentially the same result. Figure 3 shows 10×10 μm^2 negative ion maps in high lateral resolution mode (Bi^+ current: 0.4 pA) for sample B after (a) 0 s, (b) 40 s, and (c) 200 s of sputtering, which correspond to (a) the surface of the sample, (b) the interface between the oxide layer and the metallic substrate (at approximately 7 nm depth) and (c) inside the metallic substrate (at approximately 30 nm depth), respectively. The images in Fig. 3a show no regions of varying intensity, indicating the formation of a homogeneous aluminium oxide film in the near surface region. However, as the metal/oxide interface is approached, isolated areas of higher $^{63}Cu^-$ intensity, and some corresponding areas of low Al_2^- intensity are detected, becoming more pronounced with increasing sputtering time. Figure 3b shows the ion maps at the metal/oxide interface, with clear evidence for isolated Cu-rich regions. These regions are approximately the same size as the θ phase particles seen in Fig. 1; they range between 250 and 800 nm in size with a density of about 0.5 μm^{-2}. As shown in Fig. 3c, no further evidence of localized Cu enrichment was obtained on ion images after sputtering beyond the metal/oxide interface, despite the fact that the particles are through-thickness, as shown in Figs. 1b and 1c.

Figure 4 presents two ToF-SIMS negative ion depth profiles of the Al-7% Cu sample C. The profile in Fig. 4a was recorded inside the exposed area and the profile in Fig. 4b was recorded outside the exposed area. In both depth profiles, a sharp rise of the Al_2^- signal intensity is observed after 75 s sputtering, indicating a similar oxide layer thickness for treated and non-treated areas. Nevertheless, inside the treated area a gradual increase of the Al_2^- intensity signal between 75 and 500 s of sputtering and a slow decay of the AlO_2^- intensity signal indicate that, in this region, the corrosion products that are formed inside the pits dominate the profile.

Secondary electron (SE) and secondary ion (SI) images of the exact same area of sample C, both recorded from the ToF-SIMS spectrometer, are presented in Figs. 5a and 5b, respectively. Pits are clearly seen in the SE image as dark spots with a density of about 0.6 μm^{-2}. The ToF-SIMS SI maps in Fig. 5b indicate that the Si^-, O^-, AlO^- and AlO_2^- ion intensities are higher at the exact locations of the dark spots in the SE image. The higher Si^- intensity in the pits indicates that the pits have reached the SiO_2/Si substrate (white arrows). The high intensities of O^-, AlO^- and AlO_2^- ions (white arrows) suggest that the pits contain corrosion products that are mainly aluminium oxide or hydroxide, as previously stated from the

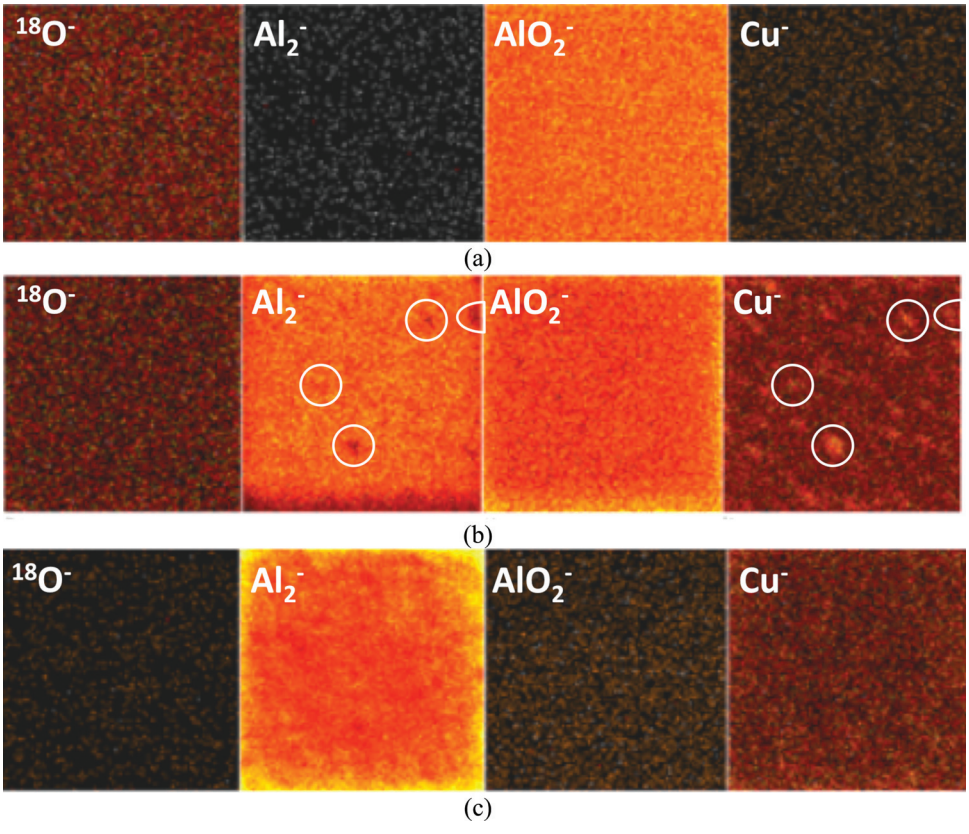

Figure 3. (Color online) ToF-SIMS negative ion images of $^{18}O^-$, Al_2^-, AlO_2^- and Cu^- recorded on the thin film Al-3.5 wt % Cu sample B after (a) 0 s, (b) 40 s, and (c) 200 s of sputtering. Regions of Cu enrichment and Al depletion are circled in (b) for clarity.

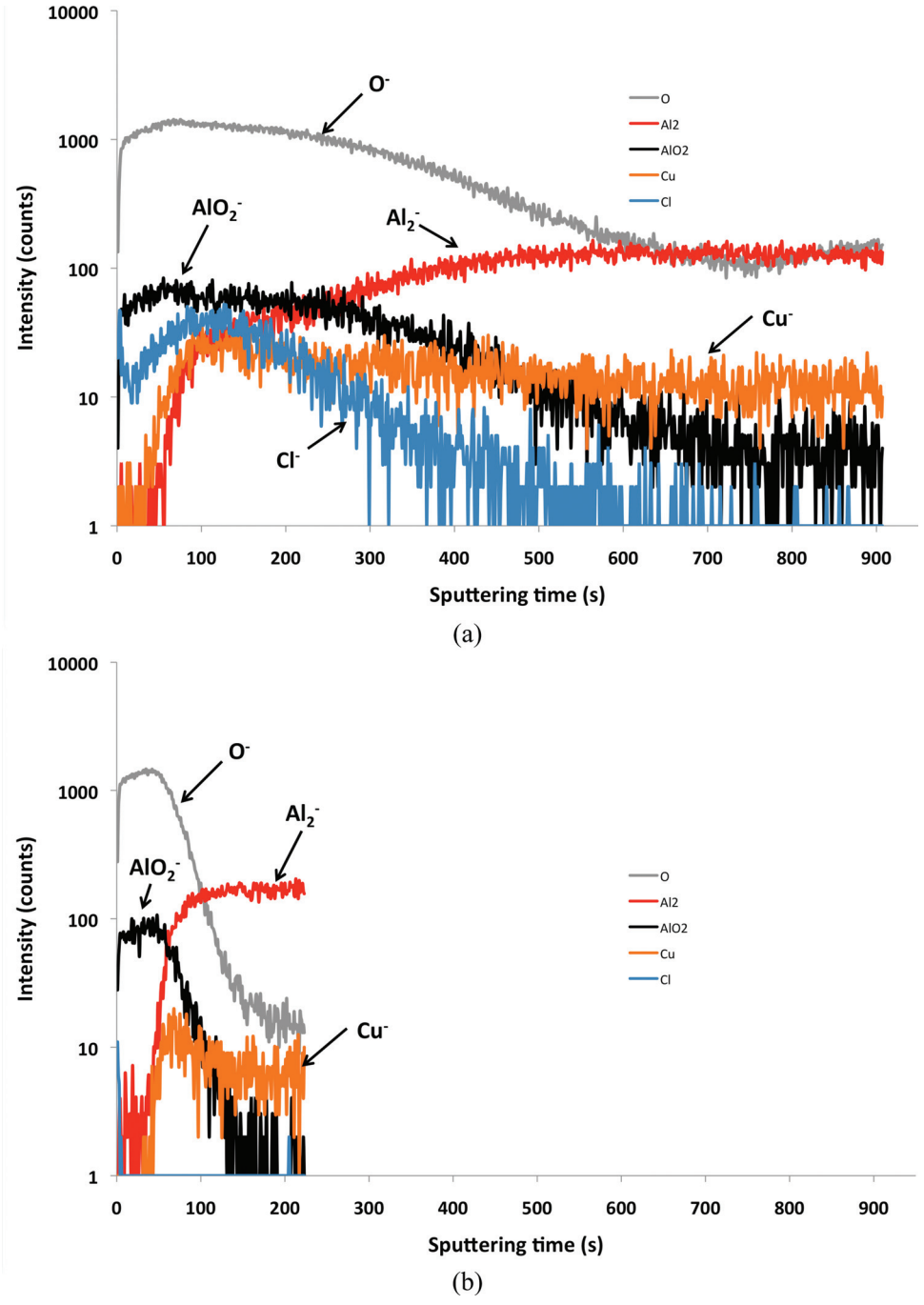

Figure 4. (Color online) ToF-SIMS negative ion depth profiles of the thin film Al-7 wt % Cu sample C. (a) Depth profile recorded inside the exposed area and (b) Depth profile recorded in an unexposed area.

examination of the depth profiles in Fig. 4. Some of the pits have slightly elevated Cu content as indicated by the $^{63}Cu^-$ image (orange arrows). This might be associated with the Al_2Cu particles or with Cu enrichment resulting from preferential dissolution of Al.

Pits with sizes ranging between 50 and 500 nm and at a density of about 3 μm^{-2} are also evident in an AFM image of the exact same area (Fig. 6). All the pits are about 15 nm deep suggesting that they do not extend to the SiO_2/Si substrate. However, as described above, the pits likely reach the substrate but contain a considerable amount of corrosion product. The higher density of pits observed with AFM compared with SI images is due to the better lateral resolution of the AFM that allows detection of pits with size lower than 150 nm (which is the lateral resolution of the ToF-SIMS spectrometer used). Nevertheless, the density of pits in the AFM image with diameter greater than 150 nm, about 0.9 μm^{-2}, is in good agreement with the density of pits detected on the SE or SI images.

Bulk sample.—The bulk sample exhibited a rougher surface as a result of the polishing procedure utilized (Fig. 7a). A dense distribution of Al_2Cu particles can be observed on the sample surface in the thermally-treated condition (a). The particles were larger than those in the thin film sample. Many were almost round with diameter about 1 μm, but many were elongated along the polishing direction, suggesting that the polishing scratches were preferred nucleation sites (recall that polishing was performed prior to the aging treatment). The FIB cross-section in Fig. 7b shows that a precipitate free zone (PFZ) existed below the surface particles. The sample was tilted by 52° in the SEM image, so the average thickness of the surface particles is about 300 nm and the depth of the PFZ is about 1.6 μm. Below the PFZ, the particles are lathe-like with crystallographic orientation. Other FIB sections (not presented) show large precipitates at subsurface grain boundaries and PFZs of similar dimensions in the grain interiors around those grain boundary particles.

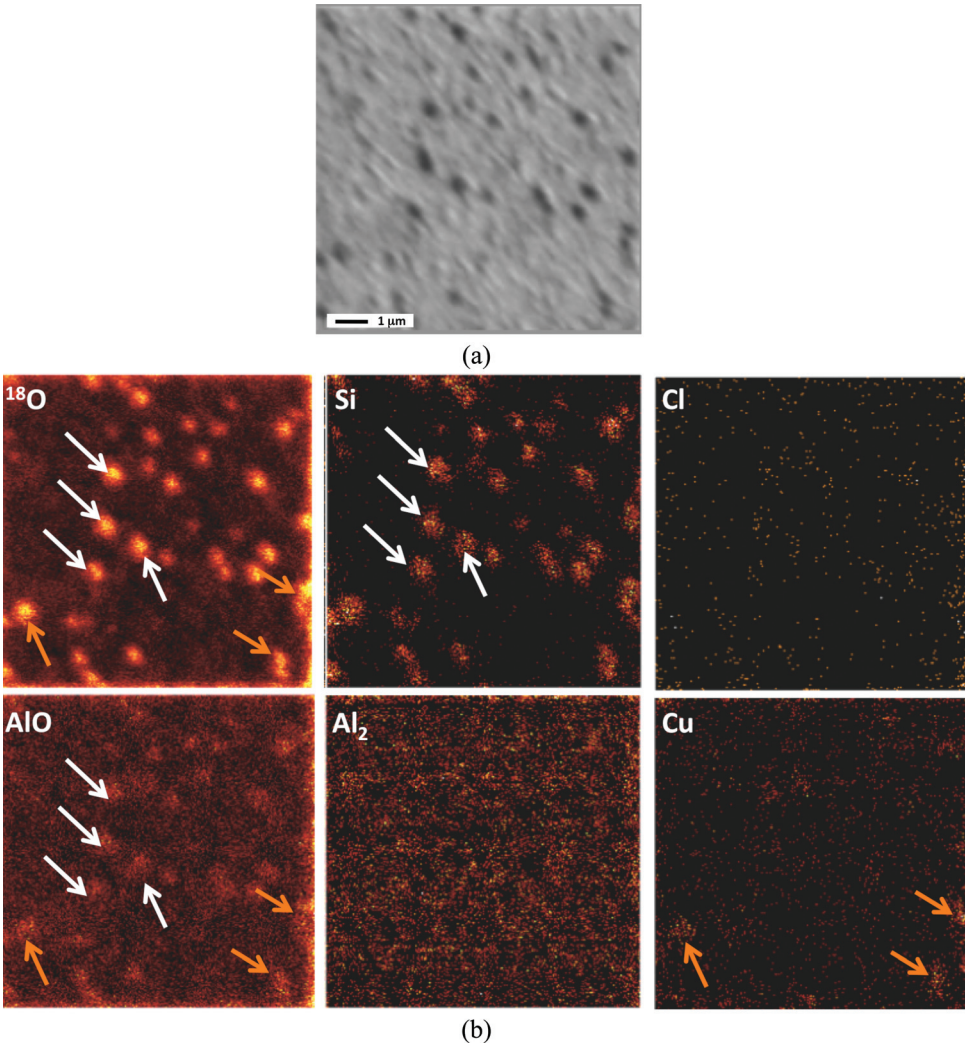

Figure 5. (Color online) Secondary electron image (a) and secondary ion images (b) recorded at the same location, showing the pits formed on the Al-7 wt % Cu sample C.

SIMS analysis was performed on this sample to investigate the ability of the ToF-SIMS mapping to identify larger θ phase particles. Figure 8 shows a ToF-SIMS negative ion depth profile of the bulk sample D. The oxide layer thickness corresponds to a Cs^+ sputtering time of ~350 s. According to the sputtering conditions used (500×500 μm^2, 47.4 nA, 0.5 keV) and to the sputter yield, the oxide layer thickness is estimated to be ~8.8 nm. ToF-SIMS mapping was performed on this sample as was done for the thin film sample. The maps at the surface indicated a homogeneous Al oxide surface, identical to the thin film sample. Figure 9a shows negative ion maps after 220 s of sputtering, which is in the region of the metal/oxide interface. Cu localization is also observed in this sample at the interface, and the Cu-rich regions are larger and elongated, similar to the shapes observed for θ phase in the SEM (Fig. 7). Figure 9b shows negative ion maps after 800 s of sputtering, which is below the region of the metal/oxide interface. Bright Cu spots are seen at the site of some of the spots seen in the 220 s maps, indicating that the ToF-SIMS technique can visualize large θ phase particles in the metal matrix. However, the boundary between the θ phase and the matrix is not very clear.

Discussion

An oxide film was formed on the surface of the Al-3.5% Cu thin films as the result of exposure of the as-deposited films to oxygen and then subsequent thermal treatment in air. The as-deposited film was likely a homogeneous solid solution of Al and Cu, which would have oxidized uniformly in the oxygen environment. Any further

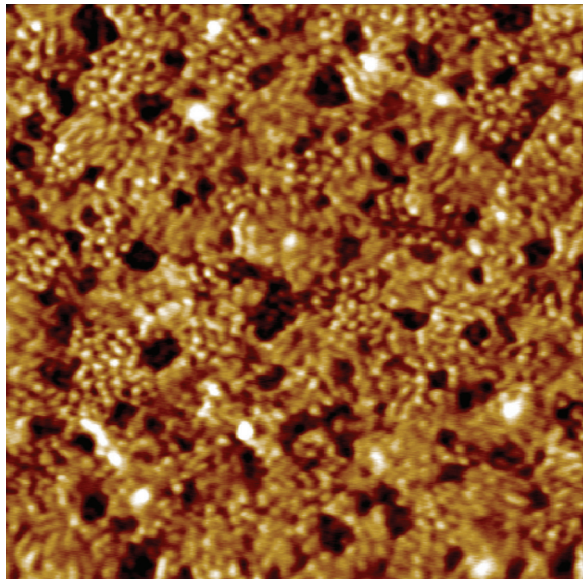

Figure 6. (Color online) Acoustic AC (AAC) AFM topographic image obtained on the Al-7 wt % Cu sample C. Pits with sizes ranging between 50 and 500 nm are clearly observed on the surface.

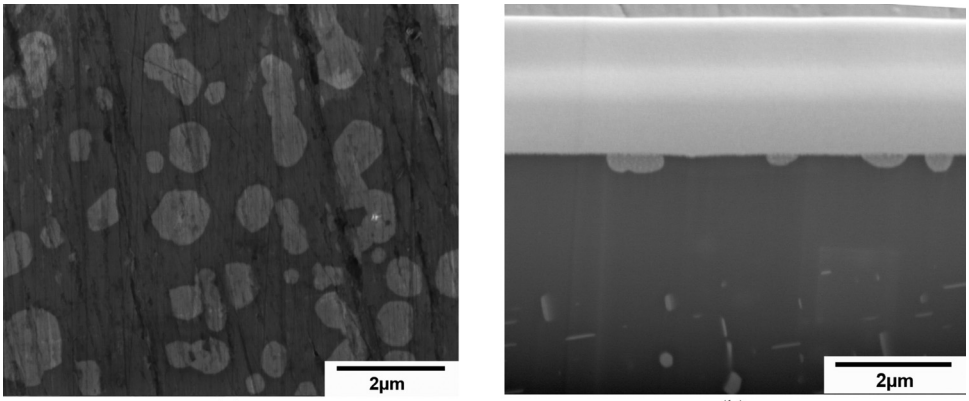

Figure 7. SEM images of bulk sample after aging treatment. (a) Top view of sample showing distribution of micron-sized Al_2Cu particles. (b) FIB cross section showing depth distribution of Al_2Cu particles with a precipitate-free zone.

oxidation during the thermal treatment happened simultaneously with the development of the microstructure to the condition of θ phase in the Cu-depleted matrix. The SIMS maps of samples in condition (a), the as-heat-treated condition, indicate that the outer part of the oxide is homogeneous Al oxide. Preferential oxidation of Al is expected, and the development of the heterogeneous microstructure did not affect the oxide composition. The SIMS depth profiles show a metallic Cu peak at the metal/oxide interface, which is likely associated with the enrichment of Cu that would result from preferential Al oxidation.

The SIMS compositional maps indicate that localized, metallic Cu-rich regions are formed at the oxide/metal interface that are approximately of the size of the θ phase particles. ToF-SIMS analyses deeper into the metal do not show localized Cu enrichment associated with the θ phase particles. This was unexpected since θ phase particles are observed by cross-sectional SEM and TEM to develop through-thickness on the Al-Cu thin films as shown in Fig. 1c. This suggests that the localized Cu enrichment at the interface is not associated with underlying θ phase particles. However, although SIMS maps in the metal show no evidence of Cu localization anywhere, it is important to note, that in the conditions used here for ToF-SIMS analyses (i.e. negative polarity), the secondary ion yield is much higher for oxide matrices than for metal matrices, so it is likely that the small θ phase particles are beyond the spatial resolution (∼150 nm) of the SIMS tool in negative polarity. The larger θ phase particles formed at the surface of the bulk Al-Cu alloy given the same heat treatment could be observed in the SIMS maps but their borders were not very distinct (Fig. 9).

Given this understanding of the limitations of the SIMS mapping, different explanations for the localization of Cu observed at the oxide/metal interface are possible. One possibility is that a heterogeneous Cu enriched layer is formed (as a result of the preferential oxidation of Al), when the as-deposited homogeneous Al-Cu thin film was exposed to oxygen. These Cu rich regions might have acted as nucleation sites for θ phase particles during the subsequent anneal or they might not have been associated with the θ phase particles; because it was not possible to observe the particles in the metal matrix, this association could not be proved for the thin films. On the other hand, the Cu enrichment at the oxide/metal interface of the bulk sample seemed to be associated with underlying θ phase particles.

An alternative explanation is that further oxidation occurred during the thermal treatment so that the heterogeneous microstructure could affect the development of the oxide/metal interface. The peak in the Cu signal at the oxide/metal interface would then result from a thinner Al oxide above the particles, with an enhancement of the ionisation of Cu in the θ phase particles at the oxide interface.

Regardless of the explanation for their formation, the localized Cu-rich regions indicate that there are local variations in the oxide

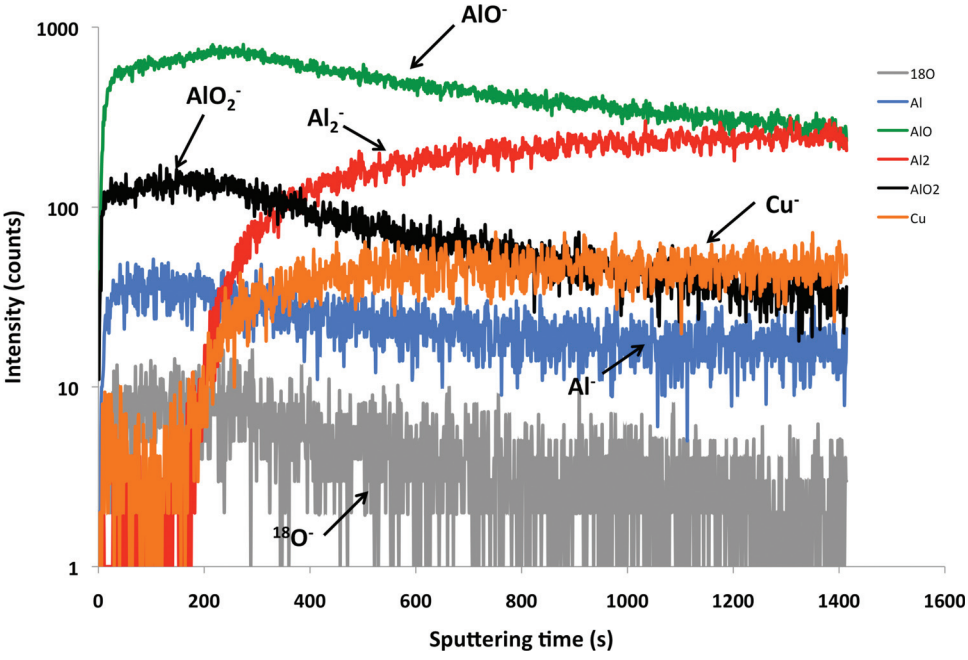

Figure 8. (Color online) ToF-SIMS negative ion depth profile obtained on the bulk Al-4 wt % Cu sample.

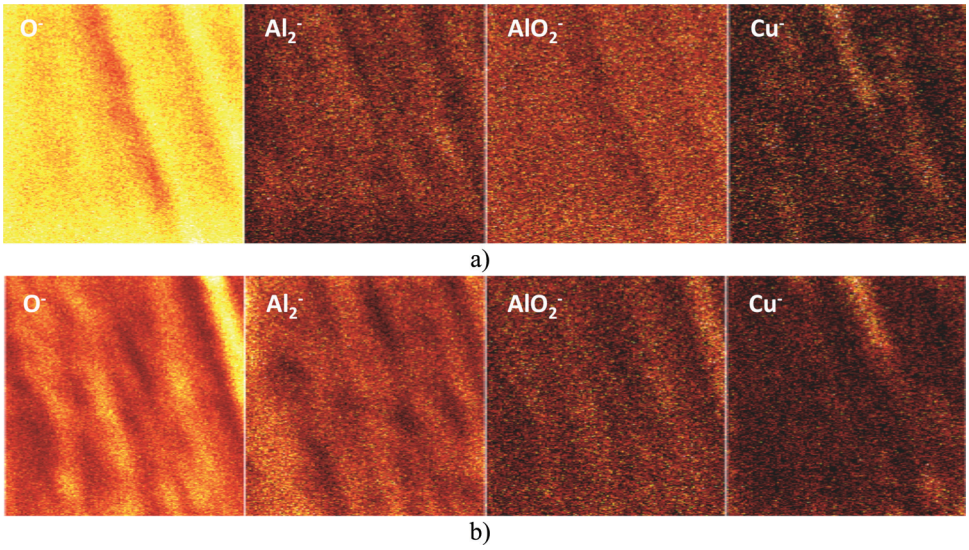

Figure 9. (Color online) ToF-SIMS negative ion images of $^{18}O^-$, Al_2^-, AlO_2^- and Cu^- recorded on the bulk Al-4 wt % Cu sample (a) after 220 s of sputtering, (b) after 800 s of sputtering.

thickness and/or interfacial composition. It is reasonable that these regions are more catalytic than areas with no Cu enrichment, so that they could be preferred sites for the cathodic reaction. Alternatively, a thinner oxide above the Cu-rich regions would likely be more susceptible to localized corrosion in a chloride environment. However, within the sensitivity of the SIMS technique, no evidence for differences in composition among Cu-rich regions was observed that could explain why attack was found only at some particles and not others during localized corrosion.

Conclusions

ToF-SIMS imaging of model thin film Al-Cu alloys showed that in the absence of localized corrosion, pure Al oxide exists above both the intermetallic Al_2Cu particles and the surrounding matrix. Depth profiling, combined with ion imaging as a function of depth, showed localized enrichment of metallic Cu at the metal/oxide interface. The size and density of these Cu-rich regions corresponded to that of the intermetallic particles. Following exposure to an aggressive environment, where localized corrosion was initiated, the pit density closely matched that of the Cu-rich interfacial regions. The locally thinner oxide in these regions could provide initiation sites for localized corrosion.

Acknowledgments

Region Ile-de-France is acknowledged for partial support for the ToF-SIMS equipment. The authors thank R. G. Copeland and J. Rivera for the Al-Cu thin film deposition, and M. Rye for the thin film SEM characterization. Sandia National Laboratories is a multiprogram laboratory operated by Sandia Corporation, a wholly owned subsidiary of Lockheed Martin company, for the U.S. Department of Energy's National Nuclear Security Administration under contract DE-AC04-94AL85000. NM's research was supported by the U.S. Department of Energy, Office of Basic Energy Sciences, Division of Materials Science and Engineering, under Contract DE-AC02-98CH1088. Financial support of GSF by the University Pierre and Marie Curie during his stay at ENSCP in Paris as guest professor is gratefully acknowledged.

École Nationale Supérieure de Chimie de Paris assisted in meeting the publication costs of this article.

References

1. J. R. Galvele and S. M. DeMicheli, *Corros. Sci.*, **10**, 795 (1970).
2. I. L. Muller and J. R. Galvele, *Corros. Sci.*, **17**, 179 (1977).
3. J. R. Scully, R. P. Frankenthal, K. J. Hanson, D. J. Siconolfi, and J. D. Sinclair, *J. Electrochem. Soc.*, **137**, 1365 (1990).
4. J. R. Scully, D. E. Peebles, A. D. Romig, Jr., D. R. Frear, and C. R. Hills, *Metall. Trans. A*, **23A**, 2641 (1992).
5. G. S. Chen, M. Gao, and R. P. Wei, *Corrosion*, **52**, 8 (1996).
6. R. G. Buchheit, R. P. Grant, P. F. Hlava, B. Mckenzie, and G. L. Zender, *J. Electrochem. Soc.*, **144**, 2621 (1997).
7. C. Blanc, B. Lavelle, and G. Mankowski, *Corros. Sci.*, **39**, 495 (1997).
8. C.-M. Liao, J. M. Olive, M. Gao, and R. P. Wei, *Corrosion*, **55**, 451 (1998).
9. R. P. Wei, C.-M. Liao, and M. Gao, *Metall. Mater. Trans. A*, **29**, 1153 (1998).
10. T. Suter and R. C. Alkire, *J. Electrochem. Soc.*, **148**, B36 (2001).
11. G. O. Ilevbare, O. Schneider, R. G. Kelly, and J. R. Scully, *J. Electrochem. Soc.*, **151**, B453 (2004).
12. O. Schneider, G. O. Ilevbare, J. R. Scully, and R. G. Kelly, *J. Electrochem. Soc.*, **151**, B465 (2004).
13. J. R. Scully, T. O. Knight, R. G. Buchheit, and D. E. Peebles, Corros. Sci., **35**, 185 (1993).
14. C.-M. Liao and R. P. Wei, *Electrochim. Acta*, **45**, 881 (1999).
15. N. Birbilis and R. G. Buchheit, *J. Electrochem. Soc.*, **152**, B140 (2005).
16. N. Birbilis and R. G. Buchheit, *J. Electrochem. Soc.*, **155**, C117 (2008).
17. M. A. Alodan and W. H. Smyrl, *J. Electrochem. Soc.*, **145**, 1571 (1998).
18. N. Missert, J. C. Barbour, R. G. Copeland, J. E. Mikkalson, *JOM*, **53**, 34 (2001).
19. M. B. Vukmirovic, N. Dimitrov, and K. Sieradzki, *J. Electrochem. Soc.*, **149**, B428 (2002).
20. A. Kelly and R. B. Nicholson, *Prog. Mater. Sci.*, **10**, 151 (1963).
21. N. Missert, R. G. Copeland, P. Kotula, J. J. Hren, and J. Rivera, Unpublished.
22. L. Lacroix, L. Ressier, C. Blanc, and G. Mankowski, *J. Electrochem. Soc.*, **155**, C131 (2008).
23. Y. Liu, P. Bailey, T. C. Q. Noakes, G. E. Thompson, P. Skeldon, and M. R. Alexander, *Surf. Interface Anal.*, **36**, 339 (2004).
24. Y. Liu, M. A. Arenas, S. J. Garcia-Vergara, T. Hashimoto, P. Skeldon, G. E. Thompson, H. Habazaki, P. Bailey, and T. C. Q. Noakes, *Corros. Sci.*, **50**, 1475 (2008).
25. H. H. Strehblow, C. M. Melliar-Smith, and W. M. Augustyniak, *J. Electrochem. Soc.*, **125**, 915 (1978).